IEEE Access
Multidisciplinary | Rapid Review | Open Access Journal

Received January 16, 2019, accepted January 31, 2019, date of publication February 8, 2019, date of current version March 4, 2019.

Digital Object Identifier 10.1109/ACCESS.2019.2898261

Millimeter Wave Cell Discovery Based on Out-of-Band Information and Design of Beamforming

YUE XIU[1], JIAO WU[2], CHAO XIU[3], AND ZHONGPEI ZHANG[1], (Member, IEEE)
[1]National Key Laboratory of Science and Technology on Communications, University of Electronic Science and Technology of China, Chengdu 611731, China
[2]College of Electrical and Computer Engineering, Seoul National University, Seoul, South Korea
[3]Qingdao Airlines, Qingdao 266000, China

Corresponding author: Zhongpei Zhang (zhangzhongpei12345@163.com)

This work was supported in part by the Natural Science Foundation of China under Grant 61831004, Grant 61571003, and Grant 61671128.

ABSTRACT Millimeter-wave (mm-wave) communication has been widely applied in the small cellular networks, and it is not difficult to find that mm-wave plays an important role in improving the capacity and data transmission rate of the 5G network systems. Nevertheless, mm-waves also have some disadvantages, such as large propagation loss and weak penetration blockage. Although the extremely high direction of the mm-wave can compensate for the propagation loss, highly directional transmissions of the mm-wave result in conventional omnidirectional transmission cell discovery schemes may fail in mm-waves; thus, we need to redesign the cell discovery scheme of mm-wave. In addition, the overhead of mm-wave cell discovery is also large. In order to reduce the overhead and provide a reasonable solution for the mm-wave base station (BS) discovery, we propose an analysis framework that utilizes out-of-band (OOB) information assistance. First, we consider the BS discovery problem as a hypothesis test problem. We analyze the statistical properties of the generalized logarithm likelihood ratio detector and study the detection performance of the detector. Through analysis and calculation, we are able to find that the OOB scheme can not only improve the detection performance but also reduce the system overhead. Then, we also analyze the performance of the OOB scheme in the case of multiple UEs. Finally, we use the angle information provided by the OOB information to predesign the mm-wave codebooks to achieve the optimal expected mode. Analysis of the simulation results demonstrates the effectiveness of the OOB information-assisted scheme.

INDEX TERMS Millimeter wave, beamforming, cell discovery, out-of-band, GLRT.

I. INTRODUCTION

Since the spectrum range of millimeter wave (mm-wave) is 30 to 300 GHz, its abundant spectrum resources have attracted widespread attention and become an important enabling technology in 5G communication [1]–[8]. Due to the high pathloss of mm-wave, it is necessary to apply beamforming techniques in base station (BS) and user equipment (UE) of mm-wave systems to achieve high coverage rate and giant system capacity. However, since the mm-wave beamwidth is different from the traditional microwave beam, the application and design of the mm-wave beam also faces many challenges and the conventional microwave cell discovery scheme fail in the mm-wave systems [9], [10]. In addition, the system overhead of mm-wave cell discovery is huge. Next, we will introduce in detail the previous research work on BS discovery.

The associate editor coordinating the review of this manuscript and approving it for publication was Chong Han.

A. BACKGROUND AND PREVIOUS WORK

In mm-wave communication system, to successfully build communication between the UEs and the BS, the following processes must be included in communication link: cell discovery, beam alignment and cell access. These processes are the basis for achieving mm-wave communication. In particular, cell discovery is essential for the establishment of communication links in any cellular system. In cell discovery, the UE is able to detect the presence of the BS. In the conventional microwave (Sub-6GHz) system and 5G system, the omnidirectional periodic reference signal (RS) is transmitted by the BS and according to statistical information of receive signal, the BS is discovered by UEs. Nevertheless,

since the beamwidth of the mm-wave is narrow, the original omnidirectional transmission scheme cannot be used for mm-wave communication systems. In other words, although the mm-wave provides high beamforming gain and a relatively high data rate, the UEs are not able to discover and synchronize with the BS. In this case, the first step of the communication link fails and the initial access will greatly limit the application of the mm-wave cellular system.

Based on the above narrative, many schemes have been proposed to solve the mm-wave BS discovery. These schemes can be divided into the following several types. In [11]–[20], proposed several cell discovery schemes based on location information from the GPS. In [11]–[14], a cell discovery scheme based on location information is proposed, which by exploiting deep learning (DL) algorithm to acquire location information and assists mm-wave communication. In [15], the cell discovery efficiency and coverage rate of the mm-wave system are tested under the assumption that the position information is known. In [16] and [17], in the real-time mm-wave cell discovery scheme, the variation of position information is established into a Markov chain model. Another scheme is based on the auxiliary beam mm-wave cell discovery scheme [17]–[20], [21] suggested a scheme for estimating the angle of arrive (AoA) and angle of departure (AoD) of mm-wave channel by designing the auxiliary beam pair, the codebook which is designed based on angle information is used to finish the cell discovery and reduce system overhead. In [22], a scheme based on cell cooperation is proposed to design the beam of the BS in the small cell and show how to use the location information provided by the macro cells. On this basis, [23] gave the compression beam selection scheme based on the auxiliary beam pair. In addition, [24]–[26] proposed a few mm-wave beam design schemes and studies the application of beamforming and precoding in cell discovery. According to [27], the multi-band auxiliary communication and multi-point coordinated propagation are proposed to apply in heterogeneous networks. In [28], based on auxiliary beam pair heterogeneous network cell discovery scheme is proposed, which uses a matched filter (MF) to detect the UEs. The system overhead of these schemes is not able to be reduced. In [29], it is acceptable to obtain that the missed detection (MD) probability of the BS detection by evaluating the SNR of the received RSs, and then a precoding scheme based on the beamwidth is proposed to realize the BS detection of the mm-wave communication. After that, by increasing the transmit power to improve the SNR of the received RSs, a multi-layer codebook scheme that can reduce the MD probability of the mm-wave system cell discovery is proposed in [30]. In [30], the fix property of the propagation time of the RS signal is utilized, and the presence of the BS is detected based on the SNR of the received signal per time period.

Based on the above discussion, we summary some shortcomings of existing solutions. First of all, due to the beamwidth of the mm-wave is too narrow, the overhead is too large, which makes it difficult for the UEs to quickly discover the BS. Second, the above papers do not consider how to use the out-of-band (OOB) information to assist mm-wave cell discovery. Although [24]–[29] consider how to use beam assisted mm-wave cell discovery, it does not give an analysis on the performance of the OOB auxiliary mm-wave BS discovery. Finally, in the case of multiple UEs, using the above scheme will result in addition of overhead of cell discovery. These have greatly limited the application of these schemes. In this paper, we present a new OOB auxiliary approach for the mm-wave BSs discovery.

B. OUR CONTRIBUTION

The recent work [31]–[33] has discussed based on the generalized likelihood ratio test (GLRT) detector mm-wave BS detection, and the author considers the detection performance when the channel is a wideband channel or a narrowband channel. Reference [34] compares the performance of cell discovery based on GLRTs with the random beamforming scheme. Based on the GLRT detector is proposed in [35] and [36], we present a mm-wave GLRT detector that exploits the statistical characteristics of mm-wave wideband sparse channel. Moreover, we analysis the statistical properties of the GLRT detector and gave the relationship between the performance of the mm-wave cell discovery and the RSs parameters.

Second, in the paper, the spatial scan time is fixed when the beamwidth is fixed. In other words, how to compromise the time overhead of the system with the performance of the BS detection. In order to reduce the scope of the search and reduce the system time overhead, we use the Q-learning to determine the time range of the UE in the Sub-6GHz system. We then design the parameters of the RS to aid mm-wave BS discovery based on the time range obtained from the OOB information. We also compared the training overhead between random beamforming and OOB information-assisted schemes.

Finally, we studied the MD probability of mm-wave cell discovery. We demonstrate the relationship between the range of angles provided by OOB information and MD probability, moreover, according to the angle range, we also give a design scheme of coodbook of mm-wave system.

C. PAPER ORGANIZATION AND NOTATION

The rest of this paper is organized as follows. In Section II, we describe the mm-wave channel model, problem formulation. In Section III, we introduce GLRT detector of cell discovery, statistic information of GLRT detector and MD probability. In Section IV we give the performance analysis of GLRT detector with OOB information in detail. In Section V, based on OOB information codebook scheme is designed. Numerical simulations are provided in Section VI. In Section VII, we conclude the paper.

Notation: The matrix is denoted as bold uppercase letters $\boldsymbol{A}$, the column vector is bold lowercase letters $\boldsymbol{a}$. Lowercase letter a and uppercase letter A indicate scalars. $\boldsymbol{A}^T$, $\boldsymbol{A}^*$ and $\boldsymbol{A}^H$ represent transpose operation, conjugate

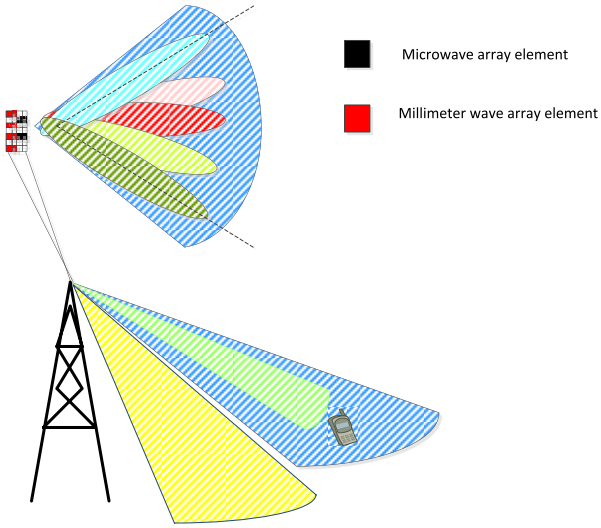

FIGURE 1. Description of the system model and beam model, the single beamformer is from the Sub-6GHz system model and the 5 beamformer are from the mm-wave system model.

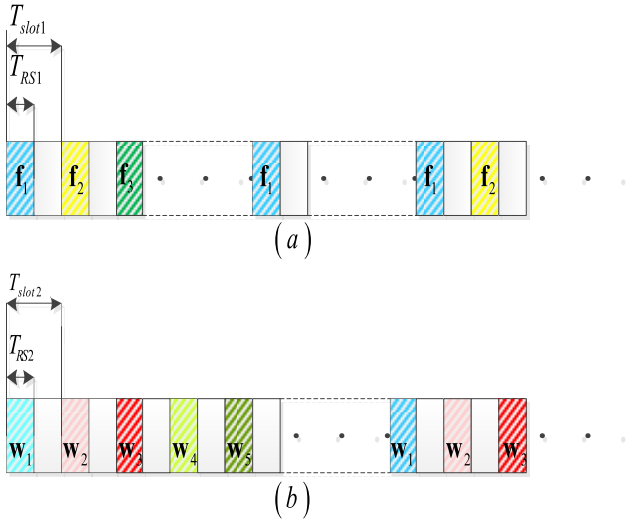

FIGURE 2. Description of the frame structure, the Fig.2(a) is frame structure of the Sub-6GHz system and Fig.2 (b) is fram structure of the mm-wave system.

operation and conjugate transpose operation, respectively. The $\boldsymbol{A}_{i,j}$ denotes the (i,j)-th entry of the matrix $\boldsymbol{A}$. The Kronecker product operation is denoted as $\otimes$. The vec($\boldsymbol{A}$) is the vector that is obtained by stacking all the columns of $\boldsymbol{A}$. The $\mathbb{R}$ and $\mathbb{C}$ are the real and complex domains, respectively. $(\cdot)^n$ is the iteration operation.

II. SYSTEM MODEL AND PROBLEM DESCRIPTION OF MM-WAVE BS DISCOVERY

Each BS in the Sub-6GHz system broadcasts the RS of the microwave spectrum and each UE within the coverage of the cell can detect the presence of the RS. In addition, we design the transmit frame structure of the microwave system. The frame structure of the Sub-6GHz system is given in Fig. 2(a), where T_{slot1} is the slot, the period of the RS signal is T_{RS1} and $T_{RS1} < T_{slot1}$. Similarly, the frame structure of the mm-wave system is given in Fig. 2(b), where T_{slot2} represents the frame structure of the mm-wave system and T_{RS1} represents the time period of mm-wave RS, $T_{RS2} < T_{slot2}$.

First, we consider the RS design of the Sub-6GHz system and the mm-wave system. In Fig.2, we give the relationship between the Sub-6GHz RS period T_{slot1} and the mm-wave RS period T_{slot2}. In this paper, we do not consider the overlap of mm-wave beams and microwave beams, considering each beam to be uncorrelated, so we can see the coverage of Sub-6GHz beam and the coverage of multiple beamformers of mm-wave are congruence and shown in Fig.1. Namely the range is roughly equal. Based on the relationship of beamwidth and the coverage rate, we can give the relationship between the two frame structures $T_{slot1} = \frac{1}{5}T_{slot2}$. To simplify this analysis process, we can give a more general expression $T_{slot1} = \frac{1}{n}T_{slot2}, m, n = 1, 2, \ldots$.

Next, we continue to considering that the mm-wave and Sub-6 GHz RSs can be directionally transmitted and repeated transmissions are performed each L_1 and L_2 slots, respectively. Specifically, as depicted in Fig.2, a series of beamformers $\boldsymbol{w}_i \in \mathbb{C}^{N_T \times 1}, i = 1, \ldots, n$ and $\boldsymbol{f}_j \in \mathbb{C}^{N_t \times 1}$, $j = 1, \ldots, m$ are utilized to transmit RS sequences in L_1 and L_2 consecutive time slots, where m denotes the number of microwave beam, N_T and N_t represent the number of mm-wave transmit antennas and Sub-6GHz transmit antennas.

According to the beam diagram given in Fig. 1, we define the spatial angular coverage of mm-wave as S_m and the spatial angle coverage of Sub-6GHz is S_{sub-6}. From the Fig.1 we can see that the wide beam S_{sub-6} is composed of several narrow beams S_m. In this paper, we consider omnidirectional transmission and directional transmission. As shown in Fig. 1, directional transmission is a special case.

We denote RS as $\boldsymbol{x}(t)$, where $\boldsymbol{x}(t) \neq 0$ and $t \in [0, T_{RS2}]$. The received signal can be expressed as

$$\boldsymbol{y}(t) = \sum_{q=-\infty}^{+\infty} z_{i\%q} \boldsymbol{H}_q \boldsymbol{w}_{i\%q} \boldsymbol{x}(t-(q-1)T_{slot}-\tau_0) + \boldsymbol{n}(t). \quad (1)$$

where $i\%q$ is modulo operation and the $i\%q = q, q \in \mathbb{Z}$ and $i = kq + l, 1 \leq l \leq J$.

Where $\boldsymbol{H}_q$ is a sparse mm-wave channel and in [14] and [24], the channel model is established by exploiting beam tracking method. To simplify the analysis, we consider the channel is a quasi-static channel, that is, the channel is unchanged in a time slot. The wideband mm-wave channel $\boldsymbol{H}_q$ in q-th slot can be expressed as

$$\boldsymbol{H}_q = \sum_{k=1}^{\kappa} \alpha_{q,\kappa} e^{-j\frac{2\pi k}{K}T_{slot}} \boldsymbol{a}_R^H(\theta_{q,k}) \boldsymbol{a}_T(\vartheta_{q,k}), \quad (2)$$

where κ is the number of multipaths and $\alpha_{q,\kappa}$ is the path gain of the κ-th path of the q-th time slot. $\boldsymbol{a}_R(\theta_{q,k})$ and

$\boldsymbol{a}_T(\vartheta_{q,k})$ represent the array response vectors of the receiver and the transmitter, respectively. Where $\theta_{q,k}$ represents AoA and AOD is expressed as $\vartheta_{q,k}$. To simplify our analysis, we only consider a uniform linear array (ULA) in this paper. If we consider a uniform phase array (UPA), we only need to increase the horizontal direction angle. The array response vector $\boldsymbol{a}_R(\theta_{q,k})$ and $\boldsymbol{a}_T(\vartheta_{q,k})$ can be expressed as

$$\boldsymbol{a}_R(\theta_{q,k}) = [1, e^{j\pi \sin(\theta_{q,k})}, \ldots, e^{j\pi(N_R-1)\sin(\theta_{q,k})}] \tag{3}$$

and

$$\boldsymbol{a}_T(\vartheta_{q,k}) = [1, e^{j\pi \sin(\vartheta_{q,k})}, \ldots, e^{j\pi(N_T-1)\sin(\vartheta_{q,k})}] \tag{4}$$

To simplify the expression (1), some parameters are implicit in the (5). This formula (1) can be rewritten as

$$\begin{aligned} \boldsymbol{y}(t) &= \sum_{q=-\infty}^{+\infty} \boldsymbol{z}\boldsymbol{H}\boldsymbol{w}\boldsymbol{x}(t-(q-1)T_{slot})+\boldsymbol{n}(t) \\ &\overset{t=t+\tau}{=} \sum_{q=-\infty}^{+\infty} \underbrace{\boldsymbol{z}\boldsymbol{H}\boldsymbol{w}}_{\boldsymbol{h}} \underbrace{\boldsymbol{x}(t-(q-1)T_{slot}+\tau-\tau_0)}_{\boldsymbol{s}} + \underbrace{\boldsymbol{n}(t+\tau)}_{\boldsymbol{n}} \\ \boldsymbol{y}_{q,\tau}(t) &= \boldsymbol{h}\boldsymbol{s}+\boldsymbol{n} \end{aligned} \tag{5}$$

where $\boldsymbol{h} = \boldsymbol{z}\boldsymbol{H}\boldsymbol{w} \in \mathbb{C}^{N_R \times N_s}$ is the effective channel, which is processed by the transmitter beamformer and the receiver combiner and N_s is the length of data stream. $\boldsymbol{s}$ is represented as the q-th slot and τ delay RSs. $\boldsymbol{n}$ is the complex Additive Gaussian White Noise (AWGN) with the mean 0 and the variance σ^2. In addition, with the application of Massive MIMO and mm-wave, the number of RF chains has greatly been reduced due to its high cost, we consider the number of RF chains to be low in this paper. In our subsequent analysis, the performance of the GLRT detector is related to the parameter N_R.

In the initial BS search phase, the UEs detect the BS by detecting the presence of the $\boldsymbol{s}$ signal and finds the time τ_0 in the time RS sequence. We assume that the UE has collected a total of Q slots data. The BS is detected based on these sampling slots. In this article, we only need to detect which time period has RSs. Based on the above assumptions, the time range is limited in $[\tau, \tau + qT_{slot}]$.

We further assume that UEs sample the received signal at rate $\frac{1}{T}$, with N_{slot} samples in each slot. T is the time period of the symbol. The time τ_0 is one of the N_{slot} time slots. The sampling matrix of the received signal can be expressed as $\boldsymbol{Y}_{q,\tau} = [\boldsymbol{y}_{q,\tau}(T), \boldsymbol{y}_{q,\tau}(2T), \ldots, \boldsymbol{y}_{q,\tau}(NT)]^T \in \mathbb{C}^{N_R \times N}$ in the slot with the length T_{slot}, in addition, $N \leq N_{slot}$ is the number of sample points of per slot of the RS. Finally, we collect the sample signal matrices from all Q slots data $\boldsymbol{Y} = [\boldsymbol{Y}_{1,\tau}(T), \boldsymbol{Y}_{l,\tau}(2T), \ldots, \boldsymbol{Y}_{L,\tau}(QT)]^T \in \mathbb{C}^{QN_R \times N}$. The sampled RSs can be represented as $\boldsymbol{S} = [s(T), s(2T), \ldots, s(NT)] \in \mathbb{C}^{1 \times N}$. According to [24], the problem model of BS detection can be expressed as the following hypothesis test problem (HTP).

$$\begin{cases} \boldsymbol{Y}_{(q,:)} = \boldsymbol{H}_{(q,:)}\boldsymbol{S} + \boldsymbol{N}, & \mathcal{H}_1 : \tau = \tau_0 \\ \boldsymbol{Y}_{(q,:)} = \boldsymbol{N}, & \mathcal{H}_0 : \tau \neq \tau_0. \end{cases} \tag{6}$$

where $\boldsymbol{Y}_{(q,:)}$ is the q-th column vector. the $\boldsymbol{N}$ is AWGN matrix. Since $\boldsymbol{H} \in C^{QN_R \times 1}$ is an effective channel matrix, it contains the transmitted signal and precoding matrix. This channel matrix $\boldsymbol{H}$ is represented as 0 when no signal is transmitted. The formula (6) is obtained by the following formula

$$\boldsymbol{S} = \begin{cases} \boldsymbol{S}, & \mathcal{H}_1 : \tau = \tau_0 \\ 0, & \mathcal{H}_0 : \tau \neq \tau_0. \end{cases} \tag{7}$$

III. GENERALIZED LIKELIHOOD RATIO TEST

As described in equation (7), we now consider to using the GLRT detector to solve the BS discovery problem. There are many unknown parameters that are correlated with the parameters of the received signal and these parameters will affect the detection performance of the GLRT detector. Next, we began to studying the GLRT detector and give the GLRT expression

$$G'_{LRT}(\tau) = \frac{\sup_{A,\sigma^2} p(\boldsymbol{Y}|\mathcal{H}_1; \boldsymbol{H}, \sigma^2)}{\sup_{\sigma^2} p(\boldsymbol{Y}|\mathcal{H}_0; \sigma^2)} \underset{\mathcal{H}_0}{\overset{\mathcal{H}_1}{\gtrless}} \eta' \tag{8}$$

where η' is a threshold value. The math expression of GLRT detector is given in the Proposition 1

Proposition 1: The GLRT detector is equivalent to

$$\begin{aligned} &G_{LRT}(\tau) \\ &= \sum_{q=1}^{QN_R} \frac{\mathrm{tr}(\boldsymbol{Y}^H_{(q,:)}\boldsymbol{Y}_{(q,:)} - \boldsymbol{S}^H(\boldsymbol{S}\boldsymbol{S}^H)^{-1}\boldsymbol{S}\boldsymbol{Y}^H_{(q,:)}\boldsymbol{Y}_{(q,:)}\boldsymbol{S}^H(\boldsymbol{S}\boldsymbol{S}^H)^{-1}\boldsymbol{S})}{\mathrm{tr}(\boldsymbol{Y}^H_{(q,:)}\boldsymbol{Y}_{(q,:)})} \\ &\underset{\mathcal{H}_0}{\overset{\mathcal{H}_1}{\gtrless}} 1 - e^{-\eta'} \end{aligned} \tag{9}$$

where $\eta = 1 - e^{-\eta'}$ is the decision threshold

Proof: See Appendix A.

Next we consider the probability distribution of the GLTR statistical variable. We can simplify the formula (9) and obtain an 2-norm expression, that is, power expression. When the received signal reaches the certain energy boundary, the GLRT detector can check the presence of RS. Since the probability distribution of the GLRT variable plays an important role in the subsequent analysis. We can see that the parameters that determine the performance of the detector are mainly the parameters of the received signal. Next, we give Lemma 2

Lemma 2: The GLRT detector is equivalent to

$$G_{LRT}(\tau) = \frac{\boldsymbol{\Xi}}{\boldsymbol{\Omega}} \sim F(x|QN_R, QN_R, N-1) \tag{10}$$

where QN_R is the first and second DoF, $N-1$ is the non-center parameter of F-distribution.

Proof: See Appendix B.

According to (6), the synchronization detector at the UE is operated as follows. The observed signal Y_τ under timing offset τ is used to evaluate the $G_{LRT}(\tau)$, which is then compared with the threshold value η. If $G_{LRT}(\tau)$ is greater than η, successful synchronization can be achieved. Otherwise, the

UE adjusts its timing offset τ, e.g., let $\tau = \tau + 1$ and re-execute the above procedure until a successful synchronization appears.

In the GLRT detector, there are two kinds of probability, namely MD probability and (false alarm)FA probability. Specifically, the synchronization between the UE and the BS is often determined according to the MD probability. In the process of GLRT detection, our goal is to minimize the MD probability. The MD probability is given in the proposition 3. In the following sections, we will analysis the expression of MD probability.

Proposition 3: The MD probability is equivalent to

$$\begin{aligned}\mathbb{P}_{MD} = e^{-\frac{N-1}{2}} \sum_{r=0}^{\infty} \frac{1}{r!}(\frac{N-1}{2})^r (1 - \sum_{i=0}^{\frac{QN_R}{2}-1} \binom{QN_R+r}{2} x^i \\ \times (1-x)^{QN_R+r-1-i}) \mathbb{P}(\mathcal{H}_1) \\ + (1 - e^{-\frac{N-1}{2}} \sum_{r=0}^{\infty} \frac{1}{r!}(\frac{N-1}{2})^r \\ \times (1 - \sum_{i=0}^{\frac{QN_R}{2}-1} \binom{QN_R+r}{2} \\ x^i (1-x)^{QN_R+r-1-i})) \mathbb{P}(\mathcal{H}_0). \end{aligned} \tag{11}$$

We assume the τ_0 obey the uniform distribution, so $\mathbb{P}(\mathcal{H}_1) = \frac{\tau_0}{T}$ and $\mathbb{P}(\mathcal{H}_0) = \frac{T-\tau_0}{T}$.

Proof: See Appendix C.

IV. MULTI-USER BS DETECTION BASED ON OUT OF BAND INFORMATION

In a real-world cellular network, the location of the UE is random, so the BS can never know the direction of the UE in advance. In order to accelerate the process, we consider that the P is the transition probability of the state and the $P = 1$ denote the UE and the current beam are matched. Since the direction of the UE is unknown, [36] and [37] suggests the traditional random beamforming scheme not only wastes a lot of system overhead, but also can seriously increase the delay and even reach the delay that the system cannot tolerate. Based on the above descriptions, in this paper we use Q-Learning to achieve microwave BS detection and according to the detection results, the signal slot index an be got.

Leveraging the OOB information is provided by Sub-6GHz, we give a based on the auxiliary beam pair MD probability analysis. In Fig.3(b), we present one conceptual example of applying the auxiliary beam pair to detect mm-wave beam direction and instruct the transmission of mm-wave beam. The transmit auxiliary beam pair can be probed by [11] gave the metric standard. Next, we introduce the detection process. The receive signal of Sub-6GHz system is written as

$$\begin{aligned}\boldsymbol{\gamma} &= \sum_{i=1}^{N} \varepsilon_i \boldsymbol{a}_r^*(\psi_i) \boldsymbol{a}_t(\eta_i) \boldsymbol{A}_t^T \boldsymbol{s}_i, \\ \boldsymbol{A}_i &= [\boldsymbol{a}_t(\omega_i - \delta), \boldsymbol{a}_t(\omega_i + \delta)] \end{aligned} \tag{12}$$

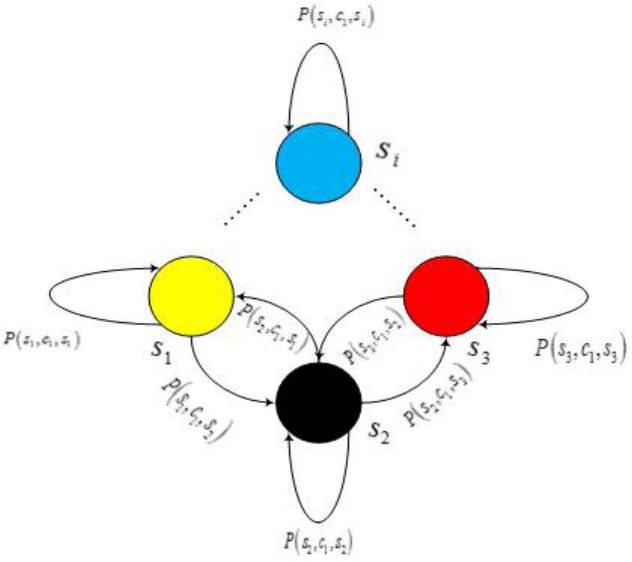

FIGURE 3. The Description of transition probabilities of beam state space of Q-Learning framework in Sub-6GHz system.

where the ε_i include the path gain and ρ is the pathloss. $\boldsymbol{a}_r(\psi_i)$ and $\boldsymbol{a}_t(\eta_i)$ denote as the receive and transmit array response vector. Due to the beamwidth is wide, we assume that the receive signal can be obtained in the angle range, we have to set two azimuth array response vectors $\boldsymbol{a}_t(\omega + \delta)$ and $\boldsymbol{a}_t(\omega - \delta)$, the azimuth array matrix is $\boldsymbol{A}_i$. In addition, we consider the transmission signal s_i is the Zadoff-Chu (ZC) sequence.

In this paper, we assumes that there are K microwave beams in the Sub-6GHz system and the set $\mathcal{K} = \{1, 2, \ldots, K\}$ of microwave beams serve a UE set $\mathcal{U} = \{1, 2, \ldots, U\}$. Our main goal is how to detect the time slot t in beam alignment of the user and the BS. We can calculate the power of the received signal, and based on the calculated power, we can infer how many mm-wave beam coverage is required for each Sub-6 GHz beam time period. Due to we consider the interference signal in the Sub-6GHz system, we can then rewrite (12) as

$$\gamma = \varepsilon_{i^*} \boldsymbol{a}_r^*(\psi_{i^*}) \boldsymbol{a}_t(\eta_{i^*}) \boldsymbol{A}_t^T \boldsymbol{s}_{i^*} + \sum_{i \neq i^*}^{N} \varepsilon_i \boldsymbol{a}_r^*(\psi_i) \times \boldsymbol{a}_t(\eta_i) \boldsymbol{A}_t^T \boldsymbol{s}_i \tag{13}$$

we consider the time-frequency synchronization of UE and BS is perfect in the paper. By utilizing the characteristics of the ZC sequence, we can further determine the power of the original signal and eliminate the interference signal. We can rewrite the expression as

$$\boldsymbol{\Xi}^{\Delta} = \sum_{i=1}^{N} s_{i_0}^* \gamma = \varepsilon_{i^*} \boldsymbol{a}_r^*(\psi_{i^*}) \boldsymbol{a}_t(\eta_{i^*}) \boldsymbol{a}_t(\omega_{i^*} - \delta) \tag{14}$$

Similarly, using the ZC sequence with the root index s_{i_1} to correlate the received signal samples,

we obtain

$$\Xi^{\Sigma} = \sum_{i=1}^{N} s_{i_1}^H \gamma = s_{i_1}^H \boldsymbol{a}_r^*(\psi_{i^*}) \boldsymbol{a}_t(\eta_{i^*}) \boldsymbol{a}_t(\omega_{i^*} + \delta) \quad (15)$$

We can calculate the corresponding received signal power as

$$\Omega^{\Sigma} = (\Xi^{\Sigma})^H \Xi^{\Sigma} = c_{\Sigma} \boldsymbol{a}_t^*(\omega_{i^*} + \delta) \boldsymbol{a}_t^*(\eta_{i^*}) \times \boldsymbol{a}_t(\eta_{i^*}) \boldsymbol{a}_t(\omega_{i^*} + \delta) \quad (16)$$

and

$$\Omega^{\Delta} = (\Xi^{\Delta})^H \Xi^{\Delta} = c_{\Delta} \boldsymbol{a}_t^*(\omega_{i^*} - \delta) \boldsymbol{a}_t^*(\eta_{i^*}) \times \boldsymbol{a}_t(\eta_{i^*}) \boldsymbol{a}_t(\omega_{i^*} - \delta) \quad (17)$$

where the c is the constant. According to [11], the downlink transmission power of microwave beam k for user u at the t-th slot is able to be expressed as

$$\gamma_{u,t} = \frac{\Omega^{\Delta} - \Omega^{\Sigma}}{\Omega^{\Delta} + \Omega^{\Sigma}} \quad (18)$$

The network state is denoted as s_t and the set of time slot is $t = \{1, 2, \ldots\}$. According to [31], we consider the transition probability of state s_t obey the Markovian property. The state s_t can be defined as

$$s_t = (\gamma_{1,t}, \gamma_{2,t}, \ldots, \gamma_{U,t}) \quad (19)$$

In fact, pathloss ρ depends on a number of parameters, including people or other surrounding obstacles and the distance between the UE and the BS. Although there is no paper to give a specific expression for ρ, the UE can detect the BS according to the formula (18) proposed in [38]–[40]. We can regard the K beams as uncorrelated beam spaces. Based on these conditions, we propose a framework for Q-learning. Q-learning is an reinforcement learning algorithm. Q-learning does not need to consider too many environment parameters and can determine the optimal strategy. In Fig.5, we present a simplified microwave BS detection scheme.

Agents: UEs $u \in U$

States: There are three possible states for the UE:1) the i-th beam and UE are matched, 2) The i-th beam transits to the right and arrives the j-th beam, and 3)The i-th beam transits to the left and arrives the j-th beam. These states are shown in Fig.3.

Action: In our problem, the network agent will decide how many UEs should be allocated to each BS. A decision c_j is chosen by UE and the c_j is the element of set $\mathcal{C} = \{c_1, c_2\}$, c_1 and c_2 denote as the UE at the current beam and switch to the other beam. When the decision $c_i \in \mathcal{C}$ is chosen by UE and the state s_t to the state s_{t+1}, the state transition probability $P(s_{t+1}|s_t, c_i)$ can be defined as

$$P(s_{t+1}|s_t, c_i) = \int_{s_{t+1}} f(s_t, c_i, s) ds, \quad (20)$$

where f denote the probability density function of state transition.

Reward: The receives rewards is denoted as $R = [R_1, R_2, \ldots, R_M]$, where R_1, R_2, R_M denote the raward when each UE at states s_1, s_2, and s_M. The rewards in all UEs $u \in \mathcal{U}$ are considered to be consistent. Due to the property of Q-learning, the convergence and the policy will be affected by reward values.

In this paper, we consider the beam state space $\mathcal{K}$ to be continuous, the action $\pi(c|s) = P(c_t = c_j|s_t = s_i)$ is considered to be extracted from the stochastic strategy $\mathcal{C}$ and it is considered a probability function of action and state. We can evaluate and improve the corresponding strategy c_i according to the value function, and the expected value of the reward in the whole process is defined as a value function. Calculate the state-value function by making the current state follow a given strategy and computing the expected value of the accumulated reward. It can be represented as

$$Q^{\pi}(s_t, c_t) = \mathbb{E}\{\sum_{t=1}^{\infty} R_t | s_t = s_i, c_t = c_j, \pi\} \quad (21)$$

where the expectation operation represents $\mathbb{E}\{\cdot\}$. The state value function $Q^{\pi}(s, c)$ is used to evaluate the benefit. The relationship between the state value function $Q^{\pi}(s_t, c_t)$ at the t time and the state value function $Q^{\pi}(s_{t+1}, c_{t+1})$ at the next time $t + 1$ is expressed as

$$Q^{\pi}(s_t, c_t) = \mathbb{E}\{R_t + Q^{\pi}(s_{t+1}, c_{t+1})\} \quad (22)$$

We can update the state value function by using iterative operation. Since the beam state space is continuous, how to choose the strategy π and the action to maximize the state value function, the goal of Q learning is to find the strategy π that can maximize the following objective function. We can summarize the algorithm table of Q learning as follows.

According to the time index that is obtained by Q-learning, we can get the angle range. According to equation (11), we can give the MD probability of multiple UEs and we can get the expression (23).

Proposition 4: The GLRT detector is equivalent to

$$\begin{aligned} \mathbb{P}_{MD} = & \sum_j \sum_i \mathbb{P}\{G_{LRT}(\tau) < \eta | \mathcal{H}_1, t_j < \tau < t_i\} \\ & \times \mathbb{P}(t_j < \tau < t_i | \mathcal{H}_1) \mathbb{P}(\mathcal{H}_1) \\ & + \sum_j \sum_i \mathbb{P}\{G_{LRT}(\tau) > \eta | \mathcal{H}_0, t_j < \tau < t_i\} \\ & \times \mathbb{P}(t_j < \tau < t_i | \mathcal{H}_0) \mathbb{P}(\mathcal{H}_0) \end{aligned}$$

Proof: The closed expression is shown in Appendix D.

V. CODEBOOK DESIGN AND BEAMFORMING

Based on index t the time interval that is detected by using Q-Learning algorithm, we can detect the angles range of UE. According to the angular range, the precoder is able to be generated and all precoders are selected as candidate precoder, that is, preset codebook can be selected in mm-wave system. Next, we discuss the design of the precoding codebook. Similarly, the method is also suitable to design the

Algorithm 1 Pseudocode for Q-Learning Algorithm

For: $t = 0, \ldots, N$ and $t = 0$ denote as the initial state
Input:Initial state $s_0 = (\gamma_{1,0}, \gamma_{2,0}, \ldots, \gamma_{U,0})$ and environment rewards R^0
1: Initial the function $Q^{\pi}(s_0, c_0)$ and c_0 is randomly select in the initial state.
For $i = 1, 2$
2: Computing the state transition probability $P(s_{t+1}|s_t, c_i) = \int_{s_{t+1}} f(s_t, c_i, s)ds$
3: Using the state transition probability to compute the Q value function
End
4:Computing Q function under the $t = t + 1$ state
5: $Q^{\pi}(s_t, c_t) = \mathbb{E}\{R_t + Q^{\pi}(s_{t+1}, c_{t+1})\}$
6: Obtain the maximum Q value function
7: Compare $\max_{\pi} Q^{\pi}(s_t, c_t)$ with $\max_{pi} Q^{\pi}(s_{t+1}, c_{t+1})$
8: while the state value function $Q^{\pi}(s_t, c_t)$ is variable
9: Continue to execute the above computation
10:Extend the strategy set $\pi = \{c_i, \ldots, c_j\}$
End
11: When the $Q^{\pi}(s_t, c_t)$ is stable
Output: the π and the iteration index t

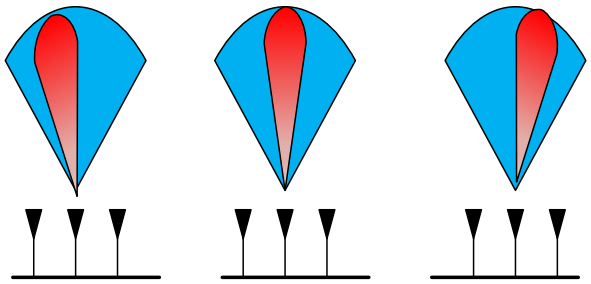

FIGURE 4. Description of the Sub-6GHz system assists mm-wave system.

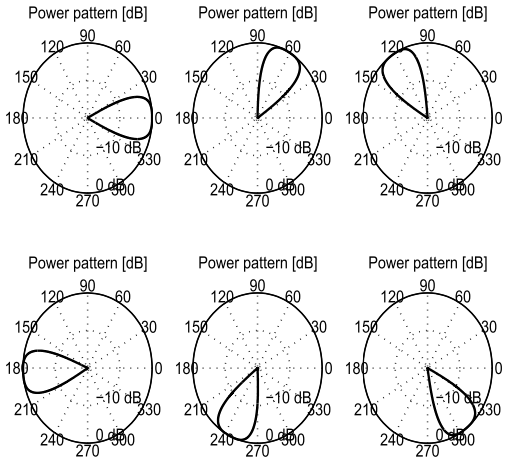

FIGURE 5. Normalized Beam pattern of Sub-6GHz system.

combined codebook, we only consider the transmitter codebook design in the paper. It is feasible to generate a precoded codebook by performing quantization operation on the array

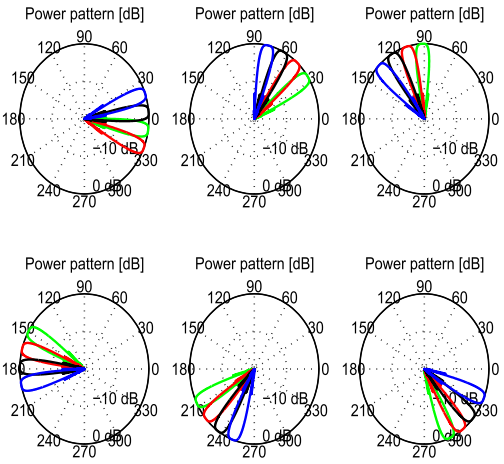

FIGURE 6. Normalized Beam pattern of quantized codebook based on OOB information in mm-wave system.

response vector of transmitter. In general, the beamwidth is produced by ULA are not equal, but according to the method proposed in [33] and [34], this method can ensure almost equal gain loss between adjacent beams. Accurate precoders require high resolution phase shifters. In this paper, we consider a β-bit phase shifter to quantize the angular extent into a set $\{0, \ldots, \frac{2\pi}{2^{\beta_{Tx}}}\}$. A quantized codebook generated by angle is provided by OOB information is shown in FIG.6. In addition, since our beam moves in the angle range $[-\pi.\pi]$, we have added a Phase shift factor with respect to time $\exp\{\frac{-t(\theta_i-\phi_i)}{2\pi}\}, \forall t \in \mathbb{N}^*$. The mm-wave beam scan pattern is shown in Fig.6.

In this paper, the transmitter has a Υ_p precoder and the receiver has a Υ_c combiner. We use w_i for the i-th precoder and z_j for the j-th combiner. $w = [w_1, w_2, \ldots, w_{N_T}]$ denotes all precoders. Similarly, $z = [z_1, z_2, \ldots, z_{N_R}]$ represents all combiners. Then we put the combiner and precoder on the phase factor. Finally, we get a time-dependent precoding $e^{\{\frac{-t(\theta_i-\phi_i)}{2\pi}\}}w$ and combiner codebook $e^{\{\frac{-t(\theta_i-\phi_i)}{2\pi}\}}z$ on the time t.

VI. NUMERICAL RESULTS

According to the formula (11), we show the variation of the MD probability with respect to SNR in Fig. 7 and Fig. 8. From the figure we can see that our proposed OOB information assist method has the best performance. This is because the OOB information provides an accurate angular range in which the mm-wave beams are concentrated in a specific area, so that there is no fluctuation in transmission power and accurate coverage of mm-waves is ensured. According to [24] and [25], omnidirectional precoding, omnidirectional combiner and random beamforming have power fluctuations in the angular direction of their transmission. In addition, this also results in performance loss due to the inability to ensure accurate beam alignment. In addition, in Fig.7 and Fig.8, we give the relationship between time overhead and MD probability of Omnidirectional combiner, omnidirectional precoding and random beamforming.

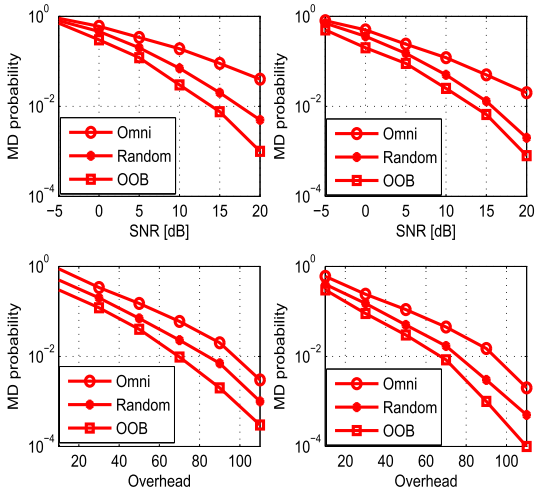

FIGURE 7. Comparsion of MD probability among proposed the OOB scheme and Omnidirectional Beamforming scheme, Random Beamforming scheme, which include the relationship of MD probability and SNR, overhead. Where the number of path $\kappa = 1$, $U = 1$.

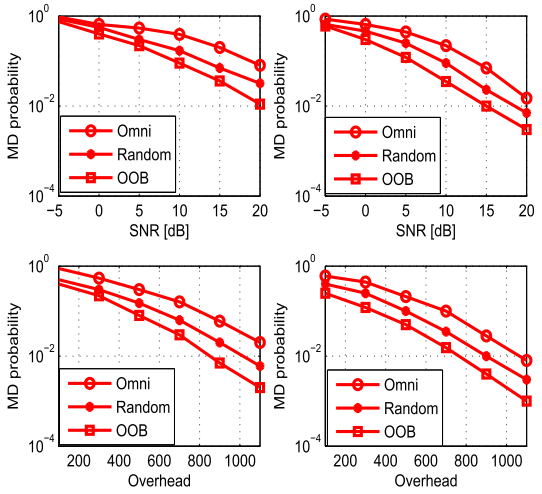

FIGURE 8. Comparsion of MD probability among proposed the OOB scheme and omnidirectional Beamforming scheme, Random Beamforming scheme, which include the relationship of MD probability and SNR, overhead. Where the number of path $\kappa = 4$, $U = 4$.

According to the formula (11), we obtain the MD probability of SNR for the above three total methods, as shown in Fig. 7 and Fig. 8. In Fig.7, we consider the number of users $U = 1$ and the number of channel paths $\kappa = 1$. It can be observed that the omnidirectional precoding scheme has very poor performance. This is mainly because it transmits narrow beams in different spatial angular directions in the t-th time slot, but since the number of channels is $\kappa = 1$, there are many time slot wastes and the beams are not aligned. This means that omnidirectional scanning wastes a lot of time overhead and the energy in the other directions is almost zero. In Method 2, the random beamforming scheme, although this method does not waste a large number of time slots like omnidirectional transmission, its performance is unstable due to the randomness of its beamforming. Moreover, although

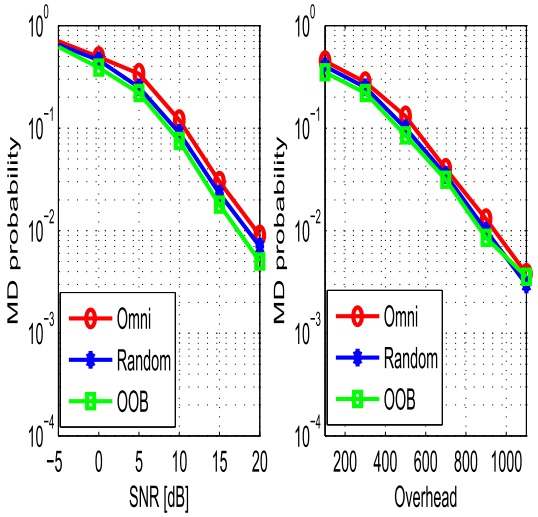

FIGURE 9. Comparsion of MD probability among proposed the OOB scheme and omnidirectional beamforming scheme, random beamforming scheme, which include the relationship of MD probability and SNR, overhead. Where the number of path $\kappa = 8$, $U = 32$.

the method can guarantee omnidirectional coverage on each time slot, when the number of channels is small, there is also a large amount of time overhead wasted. The proposed OOB assisted method, as can be seen from Fig.7, since the number of channels has been detected by the microwave spectrum, and the number of related users has also been detected. In this way we can guarantee that the beams emitted by all time slots are in a specific direction. Although there may be 2 or even more channels in the detected range of angles, the precoding scheme we have given is sufficient to ensure that each of the narrow beams and the multiple paths are aligned. In Fig.8, we find that when $U = 4$ and $\kappa = 4$, although the performance of the three methods will decrease, our performance of proposed OOB scheme is better than other schemes.

In Fig.9, we show the case which there are many users in all directions. From the results shown in the Fig.9, we can see that when the number of channels is $\kappa = 8$ and the number of users is $U = 32$, we can find the MD probabilities of the three methods are consistent at high SNR. We find that when the number of channels and the number of users increased, the performance of the three methods tends to be consistent.

In Fig.10, we consider the relationship between spectral efficiency and time overhead, SNR in a single path. For each channel, we assume that AoA and AoD are uniform distribution. In method 3, we can obtain the angular range of AoA and AoD from the OOB information, and reconstruct the transmit beamforming and receiving combination matrix by quantizing the angular range. In this paper, we use a 2-bit quantization phase shifter. As can be seen from Fig.10, the proposed OOB-assisted scheme has the highest spectral efficiency compared to several other methods. In Fig.10, we can find that as the amount of overhead increases, the spectral efficiency of the three methods tends to be stable.

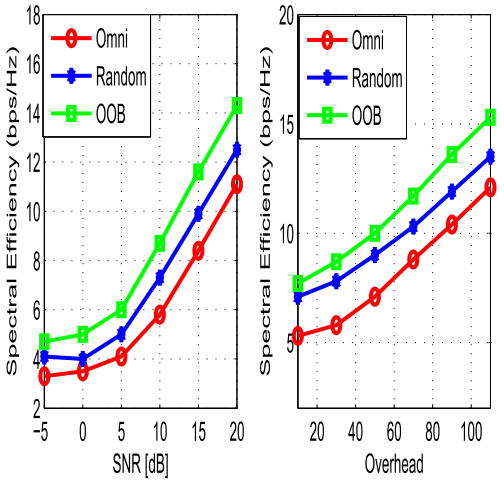

FIGURE 10. Description of the system capacity among proposed the OOB scheme and omnidirectional beamforming scheme, Random Beamforming scheme.

VII. CONCLUSION

In this paper, we propose a MD probability analysis strategy based on OOB information. In addition, we give the expression of the GLRT detector. The relationship between BS detection performance and mm-wave system parameters was established by us. Q-learning is used to obtain the OOB information. Then we analyze the OOB information-assisted detection performance under single-user and multi-user by using probability theory, and show the expected average beam pattern and the minimum average undiscovered probability in the detectable region. Finally, we designed the precoder and combiner codebook based on the range of angles provided by the OOB information. This method can flexibly adjust the mm-wave beam direction. Numerical results demonstrate the efficiency and performance of the proposed method.

APPENDIX A

A. PROOF OF THE PROPOSITION 1

Under the assumption $\mathcal{H}_1$, the probability density function (PDF) of the received signal with respect to the signal parameters can be expressed as

$$p(\boldsymbol{Y}_{(q,:)}|\mathcal{H}_1;\boldsymbol{H}_{(q,:)},\sigma^2) = \frac{1}{(\pi\sigma^2)^N}\exp\left[-\frac{\mathrm{tr}((\boldsymbol{Y}_{(q,:)}-\boldsymbol{H}_{(q,:)}\boldsymbol{S})^H(\boldsymbol{Y}_{(q,:)}-\boldsymbol{H}_{(q,:)}\boldsymbol{S}))}{\sigma^2}\right]. \tag{23}$$

Based on the sample signal, we can calculate the likelihood function as

$$L(\boldsymbol{Y}|\mathcal{H}_1;\boldsymbol{H},\sigma^2) = \prod_{q=1}^{QN_R} p(\boldsymbol{Y}_{(q,:)}|\mathcal{H}_1;\boldsymbol{H}_{(q,:)},\sigma^2)$$
$$= \frac{1}{(\pi\sigma^2)^{QNN_R}} \times \exp\sum_{q=1}^{QN_R}\left[-\frac{\mathrm{tr}((\boldsymbol{Y}_{(q,:)}-\boldsymbol{H}_{(q,:)}\boldsymbol{S})^H(\boldsymbol{Y}_{(q,:)}-\boldsymbol{H}_{(q,:)}\boldsymbol{S}))}{\sigma^2}\right]. \tag{24}$$

The logarithm likelihood function of the formula (24) can be expressed as

$$\ln L(\boldsymbol{Y}|\mathcal{H}_1;\boldsymbol{H},\sigma^2) = -QNN_R\ln(\pi\sigma^2) + \sum_{q=1}^{QN_R}\left[-\frac{\mathrm{tr}((\boldsymbol{Y}_{(q,:)}-\boldsymbol{H}_{(q,:)}\boldsymbol{S})^H(\boldsymbol{Y}_{(q,:)}-\boldsymbol{H}_{(q,:)}\boldsymbol{S}))}{\sigma^2}\right]$$
$$= -QNN_R\ln(\pi\sigma^2) + \sum_{q=1}^{QN_R}\left[-\frac{\mathrm{tr}(\boldsymbol{Y}^H_{(q,:)}\boldsymbol{Y}_{(q,:)} - \boldsymbol{Y}^H_{(q,:)}\boldsymbol{H}_{(q,:)}\boldsymbol{S})}{\sigma^2}\right] - \left[\frac{\mathrm{tr}(\boldsymbol{S}^H\boldsymbol{H}^H_{(q,:)}\boldsymbol{H}_{(q,:)}\boldsymbol{S} - \boldsymbol{S}^H\boldsymbol{H}^H_{(q,:)}\boldsymbol{Y}_{(q,:)})}{\sigma^2}\right]. \tag{25}$$

Next we find the upper bound (26), as shown at the top of the next page, of the likelihood function.

We begin to consider the logarithm likelihood function of $L(\boldsymbol{Y}|\mathcal{H}_0;\sigma^2)$

$$\sup_{\sigma^2}\ln L(\boldsymbol{Y}|\mathcal{H}_0;\sigma^2) = -QNN_R\ln(\pi\sigma^2) + \sum_{q=1}^{QN_R}\left[-\frac{\mathrm{tr}(\boldsymbol{Y}^H_{(q,:)}\boldsymbol{Y}_{(q,:)})}{\sigma^2}\right]. \tag{27}$$

According to (25)-(27), we get the final expression (28), as shown at the top of the next page. The GLRT variable is finally expressed as

$$G_{LRT}(\tau) = \sum_{q=1}^{QN_R}\frac{\mathrm{tr}(\boldsymbol{Y}^H_{(q,:)}\boldsymbol{Y}_{(q,:)} - \boldsymbol{S}^H(\boldsymbol{S}\boldsymbol{S}^H)^{-1}\boldsymbol{S}\boldsymbol{Y}^H_{(q,:)}\boldsymbol{Y}_{(q,:)}\boldsymbol{S}^H(\boldsymbol{S}\boldsymbol{S}^H)^{-1}\boldsymbol{S})}{\mathrm{tr}(\boldsymbol{Y}^H_{(q,:)}\boldsymbol{Y}_{(q,:)})} \underset{\mathcal{H}_0}{\overset{\mathcal{H}_1}{\gtrless}} 1 - e^{-\eta'}. \tag{29}$$

B. PROOF OF THE LEMMA 2

We assume the variable $\boldsymbol{\Omega}$

$$\boldsymbol{\Omega} = \sum_{q=1}^{QN_R}\|Y_{(q,:)}\|_F = \sum_{q=1}^{QN_R}\|\boldsymbol{S}\|_F\|\boldsymbol{H}_{(q,:)}\|_F + \boldsymbol{H}_{(q,:)}\boldsymbol{S}\boldsymbol{N}^H_{(q,:)} + \boldsymbol{N}_{(q,:)}\boldsymbol{S}^H\boldsymbol{H}^H_{(q,:)} + \|\boldsymbol{N}_{(q,:)}\|_F. \tag{30}$$

the $\|S\|_F = NP$ and the P is the power of signal $\boldsymbol{S}$. The $\boldsymbol{\Omega}$ can be rewritten as

$$\boldsymbol{\Omega} = \sum_{q=1}^{QN_R} NP\|\boldsymbol{H}_{(q,:)}\|_F + \boldsymbol{H}_{(q,:)}\boldsymbol{S}\boldsymbol{N}^H_{(q,:)} + \boldsymbol{N}_{(q,:)}\boldsymbol{S}^H\boldsymbol{H}^H_{(q,:)} + \sigma^2, \tag{31}$$

$$\sup_{\boldsymbol{H},\sigma^2} \ln L(\boldsymbol{Y}|\mathcal{H}_1;\boldsymbol{H},\sigma^2) - \sup_{\sigma^2} \ln L(\boldsymbol{Y}_\tau|\mathcal{H}_0;\sigma^2)$$
$$= -\ln\Big(1 - \sum_{q=1}^{QN_R} \frac{\mathrm{tr}(\boldsymbol{Y}_{(q,:)}^H\boldsymbol{Y}_{(q,:)} - \boldsymbol{S}^H(\boldsymbol{S}\boldsymbol{S}^H)^{-1}\boldsymbol{S}\boldsymbol{Y}_{(q,:)}^H\boldsymbol{Y}_{(q,:)}\boldsymbol{S}^H(\boldsymbol{S}\boldsymbol{S}^H)^{-1}\boldsymbol{S})}{\mathrm{tr}(\boldsymbol{Y}_{(q,:)}^H\boldsymbol{Y}_{(q,:)})}\Big) \underset{\mathcal{H}_0}{\overset{\mathcal{H}_1}{\gtrless}} \eta'$$
$$\triangleq \sum_{q=1}^{QN_R} \frac{\mathrm{tr}(\boldsymbol{Y}_{(q,:)}^H\boldsymbol{Y}_{(q,:)} - \boldsymbol{S}^H(\boldsymbol{S}\boldsymbol{S}^H)^{-1}\boldsymbol{S}\boldsymbol{Y}_{(q,:)}^H\boldsymbol{Y}_{(q,:)}\boldsymbol{S}^H(\boldsymbol{S}\boldsymbol{S}^H)^{-1}\boldsymbol{S})}{\mathrm{tr}(\boldsymbol{Y}_{(q,:)}^H\boldsymbol{Y}_{(q,:)})} \underset{\mathcal{H}_0}{\overset{\mathcal{H}_1}{\gtrless}} 1 - e^{-\eta'}. \tag{26}$$

$$\sup_{\boldsymbol{H},\sigma^2} \ln L(\boldsymbol{Y}|\mathcal{H}_1;\boldsymbol{H},\sigma^2) = \boldsymbol{H}_{(q,:)} = \boldsymbol{Y}_{(q,:)}\boldsymbol{S}^H(\boldsymbol{S}\boldsymbol{S}^H)^{-1} = -QNN_R\ln(\pi\sigma^2)$$
$$+\sum_{q=1}^{QN_R}\left[-\frac{\mathrm{tr}(\boldsymbol{Y}_{(q,:)}^H\boldsymbol{Y}_{(q,:)} - \boldsymbol{S}^H(\boldsymbol{S}\boldsymbol{S}^H)^{-1}\boldsymbol{S}\boldsymbol{Y}_{(q,:)}^H\boldsymbol{Y}_{(q,:)}\boldsymbol{S}^H(\boldsymbol{S}\boldsymbol{S}^H)^{-1}\boldsymbol{S})}{\sigma^2}\right]. \tag{28}$$

another variable $\boldsymbol{\Xi}$

$$\begin{aligned}\boldsymbol{\Xi} &= \sum_{q=1}^{QN_R} \mathrm{tr}(\boldsymbol{Y}_{(q,:)}^H\boldsymbol{Y}_{(q,:)} - \boldsymbol{S}^H(\boldsymbol{S}\boldsymbol{S}^H)^{-1}\boldsymbol{S}\boldsymbol{Y}_{(q,:)}^H \\ &\quad \times \boldsymbol{Y}_{(q,:)}\boldsymbol{S}^H(\boldsymbol{S}\boldsymbol{S}^H)^{-1}\boldsymbol{S}) \\ &= \sum_{q=1}^{QN_R} \|\boldsymbol{Y}_{(q,:)}\|_F - \|\boldsymbol{S}^\dagger\boldsymbol{Y}_{(q,:)}\|_F \\ &= \sum_{q=1}^{QN_R} \sigma^2 - \|\boldsymbol{S}^\dagger\boldsymbol{N}_{(q,:)}\|_F. \end{aligned} \tag{32}$$

It is easy to find that the matrix $\boldsymbol{S}^\dagger\boldsymbol{N}_{(q,:)}, q = 1,\ldots,Q$ are Gaussian distribution and $\forall i,j, \boldsymbol{S}^\dagger\boldsymbol{N}_{(i,:)}$ and $\boldsymbol{S}^\dagger\boldsymbol{N}_{(j,:)}$ are not mutually correlated. We prove that each of the variables $\boldsymbol{\Omega}$ and $\boldsymbol{\Xi}$ is the square of the Gaussian distribution and independent of each other. So the variables $\boldsymbol{\Omega}$ and $\boldsymbol{\Xi}$ are independent.

According to (31),(32), under the assumption $\mathcal{H}_1$, $\boldsymbol{\Omega}$ is a chi-square distribution with QN_R degrees of freedom (DoF) and the $\boldsymbol{\Xi}$ obeys the chi-square distribution. Finally, the GLRT statistic variable obey the F-distribution

$$G_{LRT}(\tau) = \frac{\boldsymbol{\Xi}}{\boldsymbol{\Omega}} \sim F(x|QN_R, QN_R, N-1). \tag{33}$$

C. PROOF OF THE PROPOSITION 3

The MD probability can be denoted as $\mathbb{P}_{MD} = \mathbb{P}\{G_{LRT}(\tau) < \eta|\mathcal{H}_1\}\mathbb{P}(\mathcal{H}_1) + \mathbb{P}\{G_{LRT}(\tau) > \eta|\mathcal{H}_0\}\mathbb{P}(\mathcal{H}_0)$. Since the GLRT variable is F-distributed $F(x|n_1,n_2,\lambda)$ and the sum is the probability distribution for the parameters Q, N_R, N. It is not difficult to find that $\mathbb{P}\{G_{LRT}(\tau) < \eta|\mathcal{H}_1\} \sim F(x|QN_R, QN_R, N-1)$ and $\mathbb{P}\{G_{LRT}(\tau) > \eta|\mathcal{H}_0\} \sim F(x|QN_R, QN_R, N-1)$. The PDF of non-central F-distribution is expressed as

$$\begin{aligned} f(F; QN_R, QN_R, N-1) &= e^{\frac{N-1}{2}} \sum_{r=0}^{\infty} \frac{1}{r!}\Big(\frac{N-1}{2}\Big)^r \\ &\quad \times \frac{\Gamma(QN_R + r)}{\Gamma(\frac{QN_R}{2}+r)\Gamma(\frac{QN_R}{2})} \frac{F^{\frac{QN_R}{2}-1+r}}{(1+F)^{QN_R+r}}. \end{aligned} \tag{34}$$

We can further compute the probability as $\mathbb{P}\{G_{LRT}(\tau) < \eta|\mathcal{H}_1\}$

$$\mathbb{P}\{G_{LRT}(\tau) < \eta|\mathcal{H}_1\} = \int_0^{1-e^{-\eta'}} f(F; m, n, N-1)dF,$$
$$F_a = \eta = 1 - e^{-\eta'}. \tag{35}$$

The (34) is substituted into (35)

$$\begin{aligned} &\mathbb{P}\{G_{LRT}(\tau) < \eta|\mathcal{H}_1\} \\ &= \int_0^{F_a} e^{-\frac{N-1}{2}} \sum_{r=0}^{\infty} \frac{1}{r!}\Big(\frac{N-1}{2}\Big)^r \\ &\quad \times \frac{\Gamma(QN_R + r)}{\Gamma(\frac{QN_R}{2}+r)\Gamma(\frac{QN_R}{2})} \frac{F^{\frac{QN_R}{2}-1+r}}{(1+F)^{QN_R+r}} dF \\ &= e^{\frac{N-1}{2}}\Big(\frac{N-1}{2}\Big)^r \frac{\Gamma(QN_R + r)}{\Gamma(\frac{QN_R}{2}+r)\Gamma(\frac{QN_R}{2})} \\ &\quad \times \sum_{r=0}^{\infty} \int_0^{F_a} \frac{F^{\frac{QN_R}{2}-1+r}}{(1+F)^{QN_R+r}} dF \\ &= u = Fe^{\frac{N-1}{2}}\Big(\frac{N-1}{2}\Big)^r \frac{\Gamma(QN_R + r)}{\Gamma(\frac{QN_R}{2}+r)\Gamma(\frac{QN_R}{2})} \\ &\quad \times \sum_{r=0}^{\infty} \int_0^{F_a} \frac{(u)^{\frac{QN_R}{2}-1+r}}{(u+1)^{QN_R+r}} du. \end{aligned} \tag{36}$$

$$\mathbb{P}_{MD} = e^{-\frac{N-1}{2}} \sum_{r=0}^{\infty} \frac{1}{r!} (\frac{N-1}{2})^r (1 - \sum_{i=0}^{\frac{QN_R}{2}-1} \binom{QN_R + r}{2} x^i (1-x)^{QN_R+r-1-i}) \times \mathbb{P}(\mathcal{H}_1) + (1 - e^{-\frac{N-1}{2}} \sum_{r=0}^{\infty} \frac{1}{r!} (\frac{N-1}{2})^r (1 - \sum_{i=0}^{\frac{QN_R}{2}-1} \binom{QN_R + r}{2} x^i (1-x)^{QN_R+r-1-i})) \mathbb{P}(\mathcal{H}_0). \quad (40)$$

In order to further simplify the expression (36), we give the (37)

$$B_x(p,q) = \int_0^x t^{p-1}(1-t)^{q-1} dt = \int_0^{\frac{x}{1-x}} \frac{u^{p-1}}{(1+u)^{p+q}} du. \quad (37)$$

(35) can be rewritten as

$$\begin{aligned}
&\mathbb{P}\{G_{LRT}(\tau) < \eta | \mathcal{H}_1\} \\
&= e^{-\frac{N-1}{2}} \sum_{r=0}^{\infty} \frac{1}{r!} (\frac{N-1}{2})^r \frac{B_x(\frac{QN_R}{2}+r, \frac{QN_R}{2})}{B(\frac{QN_R}{2}+r, \frac{QN_R}{2})} \\
&= e^{-\frac{N-1}{2}} \sum_{r=0}^{\infty} \frac{1}{r!} (\frac{N-1}{2})^r I_x(\frac{QN_R}{2}+r, \frac{QN_R}{2}) \\
&= e^{-\frac{N-1}{2}} \sum_{r=0}^{\infty} \frac{1}{r!} (\frac{N-1}{2})^r (1 - I_{1-x}(\frac{QN_R}{2}+r, \frac{QN_R}{2})) \\
&= e^{-\frac{N-1}{2}} \sum_{r=0}^{\infty} \frac{1}{r!} (\frac{N-1}{2})^r (1 - \sum_{i=0}^{\frac{QN_R}{2}-1} \binom{QN_R + r}{2} x^i \\
&\quad \times (1-x)^{QN_R+r-1-i}). \quad (38)
\end{aligned}$$

The $\mathbb{P}\{G_{LRT}(\tau) > \eta | \mathcal{H}_0\}$ can be denoted as

$$\begin{aligned}
&\mathbb{P}\{G_{LRT}(\tau) > \eta | \mathcal{H}_0\} \\
&= 1 - e^{-\frac{N-1}{2}} \sum_{r=0}^{\infty} \frac{1}{r!} (\frac{N-1}{2})^r \\
&\quad \times (1 - \sum_{i=0}^{\frac{QN_R}{2}-1} \binom{QN_R + r}{2} x^i (1-x)^{QN_R+r-1-i}). \quad (39)
\end{aligned}$$

Finally the $\mathbb{P}(\mathcal{H}_0)$ and $\mathbb{P}(\mathcal{H}_1)$ are determined by the number of samples. The $\mathbb{P}_{MD}$ is able to be expressed as (40), as shown at the top of this page.

APPENDIX B
PROOF OF THE PROPOSITION 4

The MD probability can be denoted as $\mathbb{P}_{MD} = \sum_j \sum_i \mathbb{P}\{G_{LRT}(\tau) < \eta | \mathcal{H}_1, t_j < \tau < t_i\} \mathbb{P}(t_j < \tau < t_i | \mathcal{H}_1) \mathbb{P}(\mathcal{H}_1) + \sum_j \sum_i \mathbb{P}\{G_{LRT}(\tau) > \eta | \mathcal{H}_0, t_j < \tau < t_i\} \mathbb{P}(t_j < \tau < t_i | \mathcal{H}_0) \mathbb{P}(\mathcal{H}_0)$. Since the GLRT variable is F-distributed $F(x|n_1, n_2, \lambda)$ and the sum is the probability distribution for the parameters Q, N_R, N. Now letars start to discuss the system probability in a concentrated case, if $\tau_0 \in (t_j, t_i)$,the $\mathbb{P}(t_j < \tau < t_i | \mathcal{H}_1) = 1$ and $\mathbb{P}(t_j < \tau < t_i | \mathcal{H}_0) = \frac{\tau - t_j}{\tau_0 - t_j}$, $\mathbb{P}(t_j < \tau < t_i | \mathcal{H}_0) = \frac{\tau - \tau_0}{t_j - \tau_0}$. When the $\tau_0 \in (t_j, t_i)$, the $\mathbb{P}(t_j < \tau < t_i | \mathcal{H}_1) = 0$ and $\mathbb{P}(t_j < \tau < t_i | \mathcal{H}_0) = \frac{\tau - t_j}{t_i - t_j}$. It is not difficult to find that $\mathbb{P}\{G_{LRT}(\tau) < \eta | \mathcal{H}_1\} \sim F(x|QN_R, QN_R, N-1)$ and $\mathbb{P}\{G_{LRT}(\tau) > \eta | \mathcal{H}_0\} \sim F(x|QN_R, QN_R, N-1)$. Finally the $\mathbb{P}(\mathcal{H}_0)$ and $\mathbb{P}(\mathcal{H}_1)$ are determined by the number of samples. If the $\tau < \tau_0$, the $\mathbb{P}_{MD}$ is able to be expressed as

$$\begin{aligned}
&\mathbb{P}_{MD} \\
&= e^{-\frac{N-1}{2}} \sum_{r=0}^{\infty} \frac{1}{r!} (\frac{N-1}{2})^r (1 - \sum_{i=0}^{\frac{QN_R}{2}-1} \binom{QN_R + r}{2} x^i \\
&\quad \times (1-x)^{QN_R+r-1-i}) \mathbb{P}(\mathcal{H}_1) + (1 - e^{-\frac{N-1}{2}} \sum_{r=0}^{\infty} \frac{1}{r!} \\
&\quad \times (\frac{N-1}{2})^r (1 - \sum_{i=0}^{\frac{QN_R}{2}-1} \binom{QN_R + r}{2} x^i (1-x)^{QN_R+r-1-i})) \\
&\quad \times \frac{\tau - t_j}{\tau_0 - t_j} \mathbb{P}(\mathcal{H}_0) \quad (41)
\end{aligned}$$

If the $\tau > \tau_0$, the $\mathbb{P}_{MD}$ is able to be written as

$$\begin{aligned}
&\mathbb{P}_{MD} \\
&= e^{-\frac{N-1}{2}} \sum_{r=0}^{\infty} \frac{1}{r!} (\frac{N-1}{2})^r (1 - \sum_{i=0}^{\frac{QN_R}{2}-1} \binom{QN_R + r}{2} x^i \\
&\quad \times (1-x)^{QN_R+r-1-i}) \mathbb{P}(\mathcal{H}_1) + (1 - e^{-\frac{N-1}{2}} \sum_{r=0}^{\infty} \frac{1}{r!} \\
&\quad \times (\frac{N-1}{2})^r (1 - \sum_{i=0}^{\frac{QN_R}{2}-1} \binom{QN_R + r}{2} x^i (1-x)^{QN_R+r-1-i})) \\
&\quad \times \frac{\tau - \tau_0}{t_j - \tau_0} \mathbb{P}(\mathcal{H}_0) \quad (42)
\end{aligned}$$

If the $\tau_0 \in (t_j, t_i)$, the $\mathbb{P}_{MD}$ is expressed as

$$\mathbb{P}_{MD} = (1 - e^{-\frac{N-1}{2}} \sum_{r=0}^{\infty} \frac{1}{r!} (\frac{N-1}{2})^r (1 - \sum_{i=0}^{\frac{QN_R}{2}-1} \times \binom{QN_R + r}{2} x^i (1-x)^{QN_R+r-1-i})) \frac{\tau - t_j}{t_i - t_j} \mathbb{P}(\mathcal{H}_0) \quad (43)$$

REFERENCES

[1] F. Boccardi, R. W. Heath, A. Lozano, T. L. Marzetta, and P. Popovski, "Five disruptive technology directions for 5G," *IEEE Commun. Mag.*, vol. 52, no. 2, pp. 74–80, Feb. 2014.

[2] P. Zhouyue and F. Khan, "An introduction to millimeter-wave mobile broadband systems," *IEEE Commun. Mag.*, vol. 49, no. 6, pp. 101–107, Jun. 2011.

[3] T. S. Rappaport *et al.*, "Millimeter wave mobile communications for 5G cellular: It will work!" *IEEE Access*, vol. 1, pp. 335–349, May 2013.

[4] C. N. Barati *et al.*, "Initial access in millimeter wave cellular systems," *IEEE Trans. Wireless Commun.*, vol. 15, no. 12, pp. 7926–7940, Dec. 2016.

[5] P. Wang, Y. Li, L. Song, and B. Vucetic, "Multi-gigabit millimeter wave wireless communications for 5G: From fixed access to cellular networks," *IEEE Commun. Mag.*, vol. 53, no. 1, pp. 168–178, Jan. 2015.

[6] M. Bennis, M. Debbah, and H. V. Poor. (2018). "Ultra-reliable and low-latency wireless communication: Tail, risk and scale." [Online]. Available: https://arxiv.org/abs/1801.01270

[7] E. Baştuğ, M. Bennis, and M. Debbah. (2014). "Living on the edge: The role of proactive caching in 5G wireless networks." [Online]. Available: https://arxiv.org/abs/1405.5974

[8] M. R. Akdeniz *et al.*, "Millimeter wave channel modeling and cellular capacity evaluation," *IEEE J. Sel. Areas Commun.*, vol. 32, no. 6, pp. 1164–1179, Jun. 2014.

[9] T. Bai and R. W. Heath, Jr., "Coverage and rate analysis for millimeter-wave cellular networks," *IEEE Trans. Wireless Commun.*, vol. 14, no. 2, pp. 1100–1114, Feb. 2014.

[10] Y. Niu, Y. Li, D. Jin, L. Su, and A. V. Vasilakos, "A survey of millimeter wave communications (mmWave) for 5G: Opportunities and challenges," *Wireless Netw.*, vol. 21, no. 8, pp. 2657–2676, 2015.

[11] D. Zhu, J. Choi, Q. Cheng, W. Xiao, and R. W. Heath, Jr. (2018). "High-resolution angle tracking for mobile wideband millimeter-wave systems with antenna array calibration." [Online]. Available: https://arxiv.org/abs/1802.03867

[12] K. Venugopal, A. Alkhateeb, N. González-Prelcic, and R. W. Heath, Jr., "Channel estimation for hybrid architecture-based wideband millimeter wave systems," *IEEE J. Sel. Areas Commun.*, vol. 35, no. 9, pp. 1996–2009, Sep. 2017.

[13] J. Singh and S. Ramakrishna, "On the feasibility of codebook-based beamforming in millimeter wave systems with multiple antenna arrays," *IEEE Trans. Wireless Commun.*, vol. 14, no. 5, pp. 2670–2683, May 2015.

[14] M. Xiao *et al.*, "Millimeter wave communications for future mobile networks," *IEEE J. Sel. Areas Commun.*, vol. 35, no. 9, pp. 1909–1935, Sep. 2017.

[15] D. Zhu, J. Choi, and R. W. Heath, Jr., "Two-dimensional AoD and AoA acquisition for wideband millimeter-wave systems with dual-polarized MIMO," *IEEE Trans. Wireless Commun.*, vol. 16, no. 12, pp. 7890–7905, Dec. 2017.

[16] G. Sommerkom, D. Hampicke, R. Klukas, A. Richter, A. Schneider, and R. Thoma, "Reduction of DoA estimation errors caused by antenna array imperfections," in *Proc. 29th Eur. Microw. Conf.*, vol. 2, Oct. 1999, pp. 287–290.

[17] M. Gerasimenko, "Cooperative radio resource management in heterogeneous cloud radio access networks," *IEEE Access*, vol. 3, pp. 397–406, 2015.

[18] F. Xu, C. Qiu, A. Guo, and C. Zhao, "Access control for software-defined heterogeneous wireless access network," in *Proc. 16th Int. Symp. Commun. Inf. Technol. (ISCIT)*, Sep. 2016, pp. 520–524.

[19] I. Kang, S. Han, and C. You, "A study on the effect of moving small cell in heterogeneous networks with interference cancellation," in *Proc. 10th Int. Conf. Ubiquitous Future Netw. (ICUFN)*, Jul. 2018, pp. 338–340.

[20] J. Wu, C. Yuen, B. Cheng, Y. Yang, M. Wang, and J. Chen, "Bandwidth-efficient multipath transport protocol for quality-guaranteed real-time video over heterogeneous wireless networks," *IEEE Trans. Commun.*, vol. 64, no. 6, pp. 2477–2493, Jun. 2016.

[21] C. Liu, M. Li, I. B. Collings, S. V. Hanly, and P. Whiting, "Design and analysis of transmit beamforming for millimeter wave base station discovery," *IEEE Trans. Wireless Commun.*, vol. 16, no. 2, pp. 797–811, Feb. 2017.

[22] S. Abu-Surra, S. Rajagopal, and X. Zhang, "Synchronization sequence design for mmWave cellular systems," in *Proc. IEEE 11th Consumer Commun. Netw. Conf. (CCNC)*, Jan. 2014, pp. 617–622.

[23] C. N. Barati *et al.*, "Directional cell discovery in millimeter wave cellular networks," *IEEE Trans. Wireless Commun.*, vol. 14, no. 12, pp. 6664–6678, Dec. 2015.

[24] X. Meng, X. Gao, and X.-G. Xia, "Omnidirectional precoding and combining based synchronization for millimeter wave massive MIMO systems," *IEEE Trans. Commun.*, vol. 66, no. 3, pp. 1013–1026, Mar. 2018.

[25] D. W. Bliss and P. A. Parker, "Temporal synchronization of MIMO wireless communication in the presence of interference," *IEEE Trans. Signal Process.*, vol. 58, no. 3, pp. 1794–1806, Mar. 2010.

[26] A. Ali, N. González-Prelcic, and R. W. Heath, "Millimeter wave beam-selection using out-of-band spatial information," *IEEE Trans. Wireless Commun.*, vol. 17, no. 2, pp. 1038–1052, Feb. 2018.

[27] Y. Wang, G. Wei, X. Pan, and Z. Shang, "Mechansim analysis and verification of out-of-band interference effects of communication station," in *Proc. Appl. Comput. Electromagn. Soc. Symp. (ACES)*, Aug. 2017, pp. 1–2.

[28] A. Ali, N. González-Prelcic, and R. W. Heath, Jr. (2018). "Spatial covariance estimation for millimeter wave hybrid systems using out-of-band information." [Online]. Available: https://arxiv.org/abs/1804.11204

[29] B. Mohammadi, J. Nourinia, C. Ghobadi, and A. Valizade, "Design of compact UWB Band Pass filter using radial stub loaded resonator and cross-shaped coupled lines with improved out-of-band performance and sharp roll-off," in *Proc. 21st Iranian Conf. Elect. Eng. (ICEE)*, May 2013, pp. 1–5.

[30] O. Semiari, W. Saad, and M. Bennis, "Joint millimeter wave and microwave resources allocation in cellular networks with dual-mode base stations," *IEEE Wireless Commun.*, vol. 16, no. 7, pp. 4802–4816, Jul. 2017.

[31] C. J. C. H. Watkins and P. Dayan, "Q-learning," *Mach. Learn.*, vol. 8, nos. 3–4, pp. 279–292, 1992.

[32] J. N. Tsitsiklis, "Asynchronous stochastic approximation and Q-learning," *Mach. Learn.*, vol. 16, no. 3, pp. 185–202, 1994.

[33] Y. Wei, F. R. Yu, M. Song, and Z. Han, "User scheduling and resource allocation in HetNets with hybrid energy supply: An actor-critic reinforcement learning approach," *IEEE Trans. Wireless Commun.*, vol. 17, no. 1, pp. 680–692, Jan. 2018.

[34] W. Zhang and T. G. Dietterich, "A reinforcement learning approach to job-shop scheduling," in *Proc. IJCAI*, vol. 95, 1995, pp. 1114–1120.

[35] J. A. Boyan and M. L. Littman, "Packet routing in dynamically changing networks: A reinforcement learning approach," in *Proc. Adv. Neural Inf. Process. Syst.*, 1994, pp. 671–678.

[36] M. Simsek, M. Bennis, and I. Güvenç, "Context-aware mobility management in HetNets: A reinforcement learning approach," in *Proc. IEEE Wireless Commun. Netw. Conf. (WCNC)*, New Orleans, LA, USA, Mar. 2015, pp. 1536–1541.

[37] A. Asheralieva, "Bayesian reinforcement learning-based coalition formation for distributed resource sharing by device-to-device users in heterogeneous cellular networks," *IEEE Trans. Wireless Commun.*, vol. 16, no. 8, pp. 5016–5032, Aug. 2017.

[38] M. Simsek, M. Bennis, and I. Güvenç, "Learning based frequency- and time-domain inter-cell interference coordination in HetNets," *IEEE Trans. Veh. Technol.*, vol. 64, no. 10, pp. 4589–4602, Oct. 2015.

[39] I. Grondman, M. Vaandrager, L. Busoniu, R. Babuska, and E. Schuitema, "Efficient model learning methods for actor–critic control," *IEEE Trans. Syst., Man, Cybern. B, Cybern.*, vol. 42, no. 3, pp. 591–602, Jun. 2012.

[40] K. G. Vamvoudakis and F. L. Lewis, "Online actor-critic algorithm to solve the continuous-time infinite horizon optimal control problem," *Automatica*, vol. 46, no. 5, pp. 878–888, May 2010.

YUE XIU received the B.S. degree from the School of Electronic and Information Engineering, Civil Aviation Flight University of China, in 2015. He is currently pursuing the Ph.D. degree with the National Key Laboratory of Science and Technology on Communications, University of Electronic Science and Technology of China.

In 2015, he joined the successive Postgraduate and Doctoral Programs at the University of Electronic Science and Technology of China. His research interests include channel estimation, compressive sensing, vehicle-to-vehicle communication, stochastic geometry, and stochastic signal process.

JIAO WU received the B.S. degree from North China Electric Power University and the M.S. degree from the National Key Laboratory of Science and Technology on Communications, University of Electronic Science and Technology of China. She is currently pursuing the Ph.D. degree with the College of Electrical and Computer Engineering, Seoul National University, Seoul, South Korea.

Her research interests include wireless communications, multi-antenna techniques, and channel estimation.

CHAO XIU graduated from the Civil Aviation University of China. He received the bachelor's degree from the Air Traffic Management Faculty. His major is about air traffic flow control, airlines operation cost management, and flight slot optimizing. He also accepted professional training of controller and dispatcher and joined the collaborative decision making improvement research. Besides, he has knowledge about informatics.

Since 2015, he has been with the Operation Control Department, Qingdao Airlines. As a dispatcher, his responsibility is about collecting the aviation information and noticing the flight crew. Due to mastering the informatics, he joined the company navigation database construction, and in that process, he accumulated fruitful knowledge on avionics and communication as well. In the company, he is pursuing the way of balancing navigation database cost and capacity. At the same time, he studies whether using 5G in aviation area is feasible or not.

ZHONGPEI ZHANG received the B.S. and M.S. degrees from the Physics Department, Sichuan Normal University, in 1990 and 1993, respectively, and the Ph.D. degree from the School of Computer and Communication Engineering, Southwest Jiaotong University, in 2000.

From 2001 to 2003, he was a Postdoctoral Fellow with the National Key Laboratory of Microwave and Digital Communication, Tsinghua University. From 2004 to 2005, he was a Postdoctoral Fellow with the University of Oulu. He is currently a Professor and a Doctoral Tutor with the University of Electronic Science and Technology of China. He has authored or co-authored over 50 journals and conference papers. His research interests include channel coding, coordinated multiple points transmission, information theory, and channel estimation.

Dr. Zhang is a Senior Member of the China Institute of Communications and a member of IEICE. He has participated in many research projects and chaired the National High-Tech Research and Development Program of China (863 Program) Coordinated Multiple Points Transmission and the National Natural Science Foundation of China Massive MIMO Channel Acquisition.